

## Effect of Normal Ageing in Bundle on the Mechanical Properties of Tempcore Treated Reinforcing Steel Rebar

Mohamed Karroum (0009-0009-7617-2099)<sup>1</sup>, Marwa A. Abbas (0009-0009-9853-7837)<sup>1\*</sup>, Ahmed Ramadan (0009-0005-9891-1527)<sup>2</sup>, Mohamed A. Gepreel (0000-0001-5223-8182)<sup>3\*</sup>

<sup>1</sup>Metallurgical and Materials Engineering Department, Faculty of Petroleum and Mining Engineering, Suez University, Suez 43521, Egypt. E-mail: Mohamed.ShKa@pme.suezuni.edu.eg

<sup>2</sup>Egyptian steel, Cairo 11835, Egypt.

<sup>3</sup>Department of Materials Science and Engineering, Egypt–Japan University of Science and Technology, New Borg El-Arab City, Alexandria 21934, Egypt. E-mail: geprell@yahoo.com

Corresponding e-mail: Mohamed.ShKa@pme.suezuni.edu.eg, geprell@yahoo.com

**Reinforcement steel rebar is produced by several ways but most importantly the tempcore process. Due to mass production in steel rolling plants, the rebars are gathered after tempcore process at a specific temperature in bundles stack in the warehouse. The bundling temperature varies from 200 to 300 °C. The rebars need relatively long time, up to one day, to reach the room temperature in the bundles stack. This work investigates the effect of prolonged ageing time on the rebars mechanical properties after the tempcore process of both ageing in bundle and designed artificial ageing. The results of mechanical properties of ageing in bundle compared to the artificial ageing were found to be in good agreement. The yield and tensile strengths were found to decrease by 6.3 and 2.1 %, respectively, due to artificial ageing. However, the elongation and the tensile to yield ratio increased by 17.6 and 4.8 % respectively.**

**Keywords:** Ageing process, Tempcore process, Reinforcing steel rebar, Microstructure, Mechanical properties

### 1 Introduction

The global demand for producing high strength steel has been raised to achieve material saving [1], [2]. High strength reinforcing steels are now produced by one of the following methods: (a) using microalloying with elements such as niobium or vanadium by which the yield strength is increased with minor alteration in the chemical composition. The rolled bars are then slowly cooled in air [3], [4], [5], [6]. (b) hot rolling followed by strain hardening of rebar steel to increase the yield strength [7]. (c) tempcore heat treatment process in which the yield strength is increased by getting a combination of tough and soft core with a hard surface [8], [9], [10].

Because of the cost of micro-alloyed rebar steel and the low ductility of work-hardened steel, the tempcore process is considered the most reliable method to obtain high strength steel [11]. Also thermomechanically treated, TMT, rebars have other advantages over conventional steel such as higher strength, ductility, corrosion resistance, bendability, fire resistance and versatility of being produced in a wide range of sizes and grades. Before entering the hot rolling mill of rebars, steel billets are reheated to around 1150 °C in the reheating furnace [12]. The rolling stands are often divided into roughing, intermediate and finishing rolling cages to reduce the billets to the final size required. Immediately after finishing the

rolling process and getting the final product dimensions, rebars enter the quenching box where it undergoes significant structural transformations. Figure.1 illustrates the tempcore process using a typical continuous cooling transformation (CCT) diagram and the final slow cooling step in the bundles stack [13]. As shown in this figure, the tempcore process has mainly three steps: (a) quenching the rebar to get martensite phase on surface, (b) self-tempering by the core heat forming tempered martensite on the surface, and (c) slow cooling of the core ending with a ferrite and pearlite structure. Therefore, controlling the tempcore process parameters is substantial to the acquired mechanical properties depending on the volume fraction of such different coexisting phases.

During the quenching step, the rebar undergoes a designed fast cooling with specific water volume, water pressure and cooling time [15], [16]. The cooling parameters depend on the rebar diameter, speed and entrance temperature and the diameter of cooling pipe [17], [18]. The surface layer of the rebar is transformed from austenite to martensite [19]. The depth of formed martensite layer is controlled to get specific mechanical properties [20]. In the subsequent step, the rebar leaves the quenching box with a temperature gradient between its surface layer and the core. The heat transfers from the core to the surface leading to tempering the formed martensite layer [21]. Finally, in the third stage, the rebar reaches the cooling bed

where its core is slowly cooled so the austenite in the core transforms to ferrite and pearlite [22]. A mixture of bainite, ferrite and pearlite coexist in the intermediate zone between the core and the surface depending on the cooling rate through the rebar's cross section.

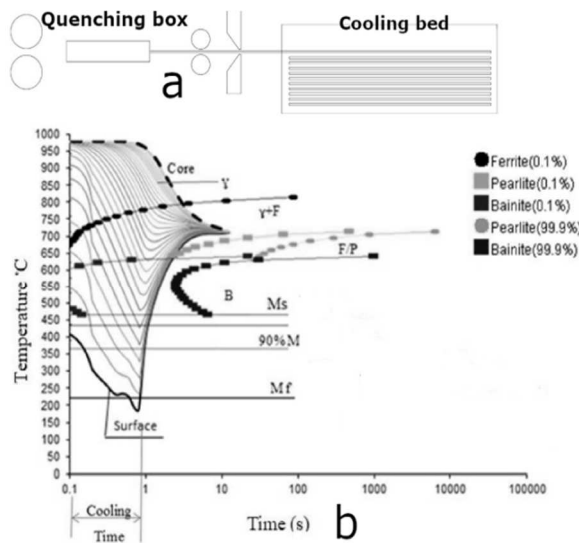


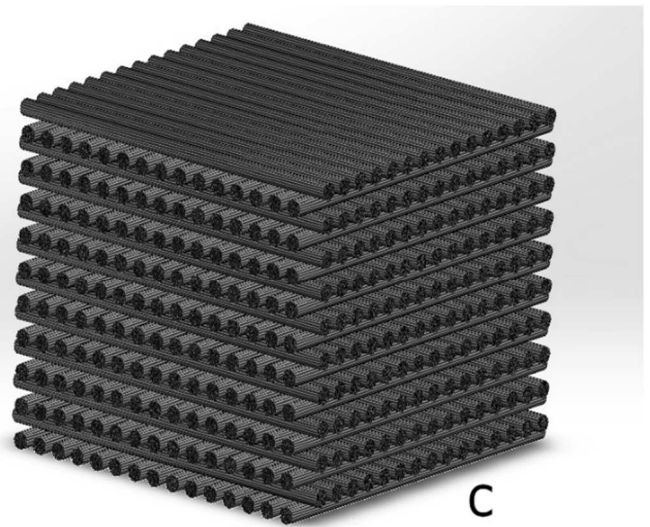
**Fig. 1** Schematic representation of tempcore process, (a), typical continuous cooling transformation (CCT) diagram during tempcore process of steel rebar followed by slow cooling of the core [14] (b), and final slow cooling stage in the bundles stack (c)

After finishing the tempcore process, the steel rebars are left to cool down from 200–300 °C to room temperature in warehouse. Due to mass production, the produced rebars are gathered in bundles, each bundle weighs 2 tons approximately which are stacked together in the plant warehouse. In practice, the bundle temperature ranges from 200–300 °C. This makes the TMT rebars cool to room temperature after prolonged periods reaching 24 hours.

Various studies have investigated the phases formed and the mechanical properties induced during the tempcore process of rebars. Different tools were elaborated, including machine learning models such as artificial neural networks [23] along with other simulation programs such as JMatPro [1], [14]. A decrease in the yield and tensile strength in of TMT steel was observed at a tempering temperature above 500 °C or after the third stage of tempering [11].

The microstructure of tempered martensite changes due to tempering and ageing. The martensite produced due to the quenching of austenite is unstable and providing a driving force for many phenomena. As-quenched martensite's extremely high dislocation density provides locations for carbon atom segregation and carbide formation encouraging recovery and recrystallization [24]. Supersaturation of carbon and alloying elements inside martensite crystals occurs due to the lack of diffusion encouraging segregation and carbide precipitation [25], [26]. A number of steps are involved in martensite tempering. First-step tempering takes place between 80 and 200 °C, during which

This in turn leads to a hard surface layer due to tempered martensite, a soft core due to ferrite and pearlite and an intermediately hardened zone due to the mixture of bainite, ferrite and pearlite.



time carbon atoms segregate and redistribute into lattice defects such as prior- $\gamma$  grain boundaries, lath boundaries, and dislocations. Furthermore, during this tempering step, the transitional epsilon-carbides ( $\epsilon$ -Fe<sub>2.4</sub>C) also formed [27], [28], [29]. In the second-step tempering (200–300 °C), retained austenite transforms into ferrite ( $\alpha$ ) and cementite ( $\theta$ -Fe<sub>3</sub>C). Stable carbides like cementite (Fe<sub>3</sub>C) form in the third step tempering (250–350 °C) [29]. Higher than 350 °C, the cementite becomes globular and coarser [29].

However, the ageing of TMT steel, after bundling, at temperatures from 200 to 300 °C down to room temperature for prolonged time has been overlooked in literature. This work is aiming to shed light and investigate the consequences of such practice on the final structure and mechanical properties using JMatPro software along with artificial ageing experiments simulating the real practice in a rebar steel plant warehouse.

## 2 Experimental procedures

TMT steel rebars are bundled at a temperature from 200 to 300 °C depending on process factors such as steel grade and diameter, rolling speed and cutting to length cycle. To estimate the change in mechanical properties due to the ageing of TMT steel rebar, six sets of specimens (10, 12, 16, 18, 22, 25 mm in diameter) were taken before the ageing. Each set was 3 specimens with length of one meter from the same bars. Then sets were left to cool down at air from 200–300 °C to room temperature. The bundles, from

which samples were taken, were put in the warehouse to cool down slowly in the bundle stack from 200-300 °C to room temperature. After that other similar six sets of specimens were taken from the same previous bars after the ageing. Then all sets were tensioned and all results were recorded.

**Tab. 1** Chemical composition of the rebar steel used in the artificial ageing

Diameter (mm)	Grade	C	Si	Mn	P	S	Cr	Ni	Cu	C Eq
18	B500DWR	0.30	0.22	1.00	0.027	0.024	0.10	0.13	0.57	0.54

For this artificial ageing procedure, a 13 m long steel rebar (18 mm diameter) was immediately segregated after exiting the cooling bed at a temperature 370 °C. The bar was immediately cut into 13 smaller bars (1 m each). 3 bars were air cooled down to room temperature. The other 10 bars were put into the heat

Another experiment of artificial ageing in heat treatment furnace was conducted on TMT rebar of 18 mm in diameter and of chemical composition given in table 1 to estimate the effect of ageing precisely and accurately.

treatment furnace held at 200 °C. Each two hours, two bars were taken out of the furnace. Bars temperature was measured at each step as shown in Figure 2. The artificially aged samples were designated as shown in table 2.

**Tab. 2** The designation of samples artificially aged at heat treatment furnace

Sample Code	Ageing time, h					
	0	2	4	6	10	24
	SNA	SA02	SA04	SA06	SA10	SA24

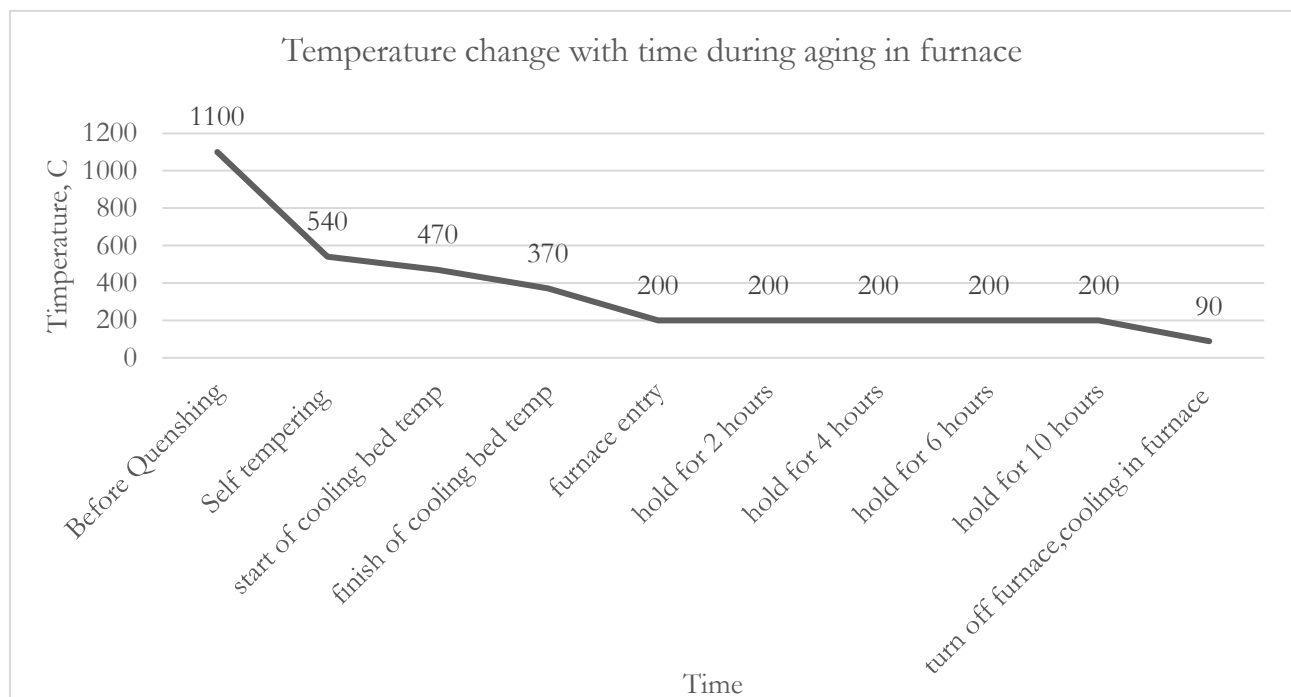


**Fig. 2** Record of Temperature during Tempcore process and the followed artificial ageing in heat treatment furnace

The tensile properties at room temperature were carried out according to ISO6892 using a WANCE HUT206D tensile machine with 1500 KN capacity. Tensile specimens were tensioned as produced with length of 50 cm. the hardness was measured using Shimadzu micro-Vickers hardness under the load of 500 gf.

JMat-Pro, thermodynamic simulation software, calculates a wide range of materials properties for alloys and is particularly aimed at multi-components alloys used in industrial practice. Using JMatPro, calculations for stable and metastable phase equilibrium, solidification behavior and properties, mechanical properties and phase transformations.

Scanning electron microscopy (SEM) and energy dispersive spectroscopy (EDS) were carried out using a FEI Inspect S50 machine equipped with a bruker AXS -flash detector 410-M. the surface of samples was polished down to 0.3  $\mu\text{m}$  using alumina suspension and then chemically polished using a 0.04  $\mu\text{m}$  colloidal suspension of silica.

### 3 Results

#### 3.1 Ageing in bundle

The measured mechanical properties for all rebar diameters before and after cooling in bundle are recorded in table 3. It is found that both yield and tensile strength values decreased due to ageing in bundle while elongation increased.

**Tab. 3** The effect of aging in bundle cooling on yield strength, tensile and elongation strength for steel bars with different sizes

Bar Size (mm)	Before bundling			After cooling in bundle			Difference		
	Yield MPa	Tensile MPa	Elongation %	Yield MPa	Tensile MPa	Elongation %	Yield MPa	Tensile MPa	Elongation %
10	573 ( $\pm 6$ )	712 ( $\pm 3$ )	23 ( $\pm 1$ )	536 ( $\pm 4$ )	694 ( $\pm 3$ )	25 ( $\pm 1$ )	-37	-18	2
12	575 ( $\pm 4$ )	667 ( $\pm 3$ )	20 ( $\pm 1$ )	536 ( $\pm 3$ )	642 ( $\pm 2$ )	22 ( $\pm 0.5$ )	-39	-25	2
16	555 ( $\pm 3$ )	657 ( $\pm 1$ )	19 ( $\pm 0.5$ )	529 ( $\pm 2$ )	647 ( $\pm 3$ )	22 ( $\pm 1$ )	-26	-10	3
18	565 ( $\pm 1$ )	661 ( $\pm 2$ )	21 ( $\pm 1$ )	545 ( $\pm 2$ )	650 ( $\pm 2$ )	23 ( $\pm 1$ )	-20	-11	2
22	576 ( $\pm 2$ )	669 ( $\pm 2$ )	18 ( $\pm 0.5$ )	548 ( $\pm 1$ )	648 ( $\pm 1$ )	21 ( $\pm 0.5$ )	-28	-21	3
25	591 ( $\pm 2$ )	751 ( $\pm 3$ )	16 ( $\pm 1$ )	568 ( $\pm 2$ )	735 ( $\pm 2$ )	18 ( $\pm 0.5$ )	-23	-16	2

#### 3.2 Artificial ageing in heat treatment furnace

##### 3.2.1 Tensile testing

The mechanical properties of 18 mm steel rebar samples (SNA, SA02, SA04, SA06, SA10, SA24) are recorded as shown in table 4. The yield strength of

SNA sample is 586 MPa whereas the yield strength of SA10 sample is 549 MPa. It can be shown that the yield strength and tensile strength decrease through aging time whereas the elongation and the tensile to yield ratio increase.

**Tab. 4** The mechanical properties of artificially aged samples

Sample code	Yield strength (YS) MPa	Tensile strength (TS) MPa	Total Elongation %	Tensile to yield ratio
SNA	586 ( $\pm 3$ )	726 ( $\pm 4$ )	17 ( $\pm 0.7$ )	1.24 ( $\pm 0.02$ )
SA02	562 ( $\pm 3$ )	719 ( $\pm 3$ )	18 ( $\pm 0.5$ )	1.28 ( $\pm 0.01$ )
SA04	556 ( $\pm 2$ )	718 ( $\pm 2$ )	18.5 ( $\pm 0.5$ )	1.29 ( $\pm 0.01$ )
SA06	560 ( $\pm 2$ )	720 ( $\pm 2$ )	18.5 ( $\pm 0.5$ )	1.29 ( $\pm 0.01$ )
SA10	549 ( $\pm 1$ )	711 ( $\pm 1$ )	20 ( $\pm 0.3$ )	1.30 ( $\pm 0.01$ )
SA24	555 ( $\pm 1$ )	718 ( $\pm 1$ )	19 ( $\pm 0.3$ )	1.29 ( $\pm 0.01$ )

##### 3.2.2 Prediction of the effects of ageing process on the core and surface layer of TMT steel rebar by JMatPro® simulation software

Prediction the equilibrium phases and precipitations foremed in the core of TMT steel rebar.

JMatPro software [30] was applied on the 18 mm tested sample in order to predict the equilibrium phases, the amount of each phase and chemical composition of predicted phases at low temperatures. The

output from the program shows the different phases at different temperatures as illustrated in Figure. 3.

MnS starts to form during solidification when the temperature is lowered below 1439 °C, as MnS becomes stable phase at all temperature ranges. At temperature below 784 °C. ferrite starts to form whereas Cementite forms below 709 °C, Copper precipitates below 690 °C, Metal phosphide, M2P, forms below 409 °C and M7C3 forms below 384 °C.

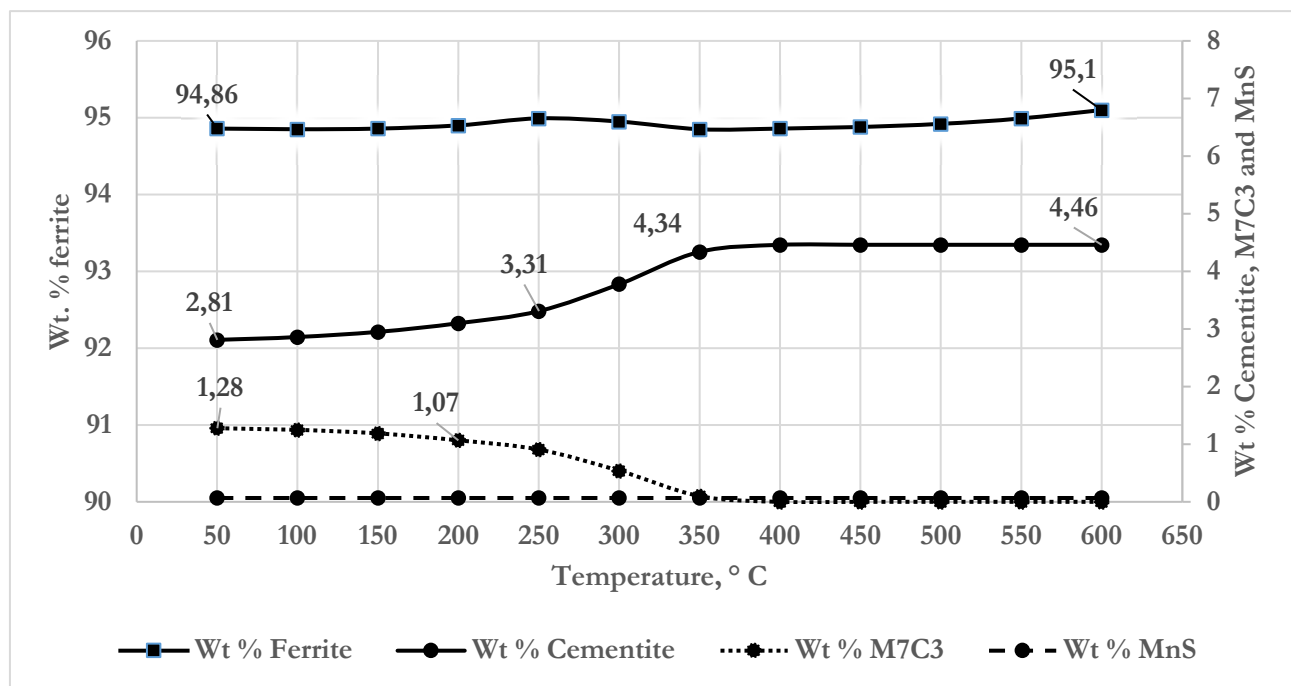


**Fig. 3** Predicted phases and precipitates at different temperatures (A) all phases and precipitates and (B) all phases and precipitates except ferrite

The weight percent of ferrite, MnS, metal nitride, MN, and copper hasn't changed much with cooling from 400 °C to room temperature. Whereas the weight percent of cementite and M7C3 has changed much with cooling from 400 °C to room temperature. M7C3 and M2P formed at temperature around 400 °C and G-phase formed at 260 °C. the amount of ferrite

is nearly constant upon cooling from 400 °C to room temperature. The amount of cementite decreases from 4.46 % at 400 °C to 2.81 % at room temperature. On the opposite side, the amount of M7C3 starts to form at 384 °C to reach 1.28 % at room temperature as shown in figure 3.

**Tab. 5** The chemical composition of predicted Cementite and M7C3 at different temperatures for tested steel

Element, wt. %		Cementite					
		Temperature, ° C					
		400	350	300	200	100	50
	Fe	74.5	73.5	75.1	80.4	85.4	87.7
	Mn	17.6	18.6	17.3	12.4	7.6	5.4
	C	6.7	6.7	6.7	6.7	6.7	6.7
	Cr	1.2	1.1	0.9	0.6	0.4	0.3
Element, wt. %		M <sub>7</sub> C <sub>3</sub>					
		Temperature, ° C					
		400	384	300	200	100	50
	Mn		38	46.3	49.8	55.3	59.4
	Fe		18.9	20.1	20.6	20.7	20.7
	C		8.1	8.5	8.5	8.5	8.5
	Cr		0.9	1.6	1.3	0.8	0.5
	Mo		30.5	17.7	12.9	11.7	11.5

The chemical composition of predicted phases and precipitates is shown in table 5 to know why the amount of each phase or precipitate changes. The

manganese amount in cementite at 400 °C is 17.58 wt. % and it decreases until it reaches 5.39 wt. % at room temperature, whereas M7C3 starts to form at 384 °C

with an amount of manganese equals 38.00 % and it increases until it reaches 59.42% at room temperature. So, we can say that manganese leaves cementite to form M<sub>7</sub>C<sub>3</sub>.

### 3.2.3 Predicting the yield strength of tempered martensite formed on the TMT steel rebar surface after tempering /ageing

The yield strength of martensite decreases with in-

creasing tempering temperature and increasing tempering time as shown in figure 4. The predicted yield stress of SNA sample (after 10 minutes) is 1617 MPa while for the SA10 sample (after 600 minutes) is 1535 MPa.

The decrease in yield strength of martensite leads to decrease in yield strength of quenched and self-tempered steel rebar. This may explain the deterioration in yield and tensile strength due to ageing.

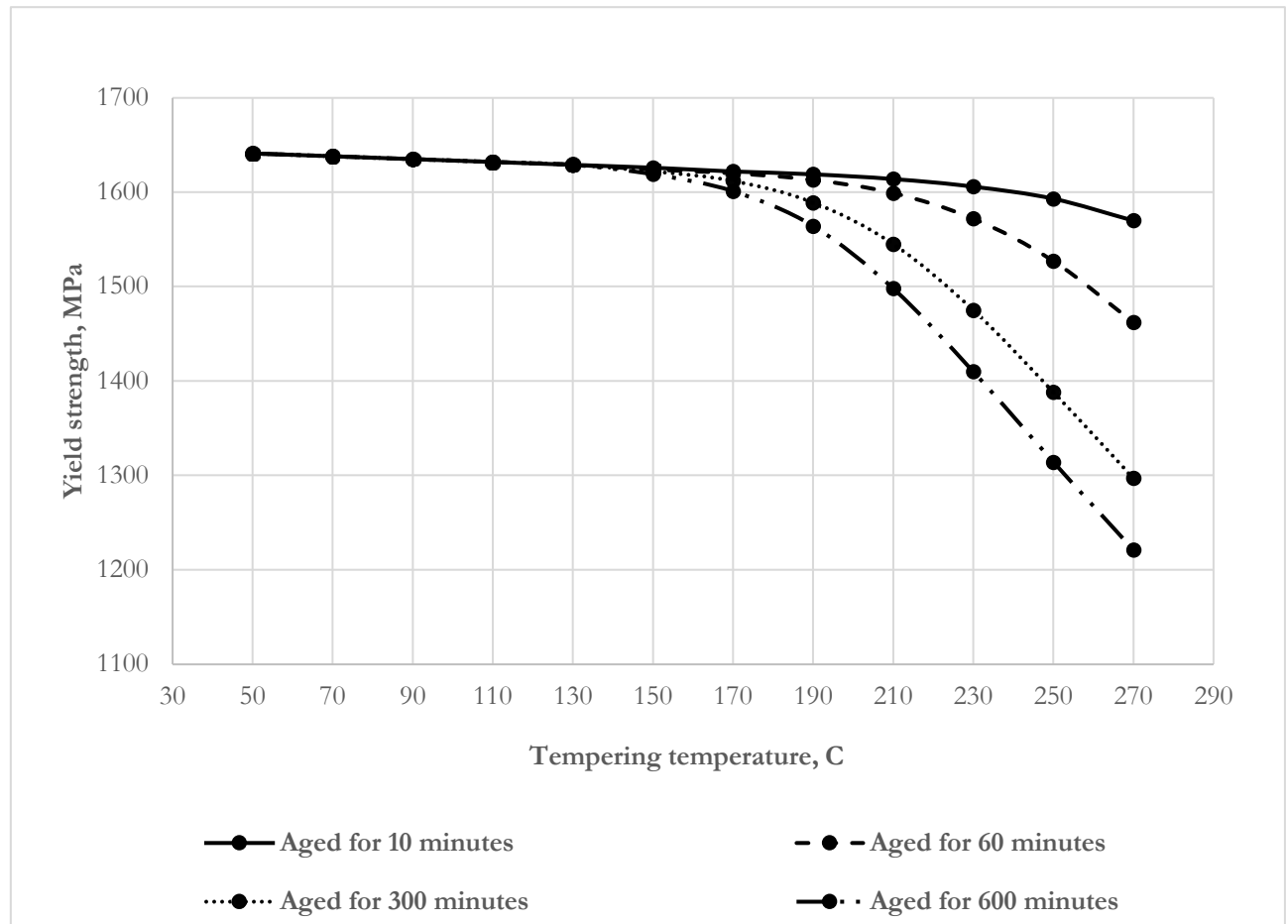


**Fig. 4** The effect of tempering temperature and tempering time on the yield strength of martensite using JMatPro® software

### 3.2.4 Metallography

The SEM micrographs of the core and the surface of SNA and SA10 samples are shown in figure 5. The core microstructures of both samples, figure 5 A and B, consist of ferrite and pearlite where the large darker areas correspond to proeutectoid ferrite. The surface microstructures, figure 5 C and D, of both samples show areas of tempered martensite. No significant difference was observed in the microstructures of SNA and SA10 samples. This shows that ageing at 200 °C did not result in a significant change in the microstructure of TMT low carbon steel [31].

The core micrographs of both SNA and SA10 samples showed some precipitates. The EDX analysis of such precipitates, table 6 and table 7, revealed their chemical composition which comply with MnS. It was also found that carbon and manganese segregate from

the matrix to precipitate around MnS precipitates. The carbon and manganese contents around MnS precipitates in SA10 sample were larger than that in SNA sample. This shows that ageing at 200 °C for 10 h provides the sufficient temperature and time for manganese carbide to form around MnS precipitates.

SNA sample was air cooled from 200 °C to room temperature after quenching and self-tempering. Such relatively fast cooling can make Mn and C combine together forming Manganese carbide precipitates which prefer locating in the matrix than around MnS precipitates. However, the SA10 sample was aged at 200 °C for 10 h after Quenching and self-tempering, then cooled to room temperature. During that prolonged time, manganese carbide precipitates preferred locating around MnS precipitates over than in the matrix.

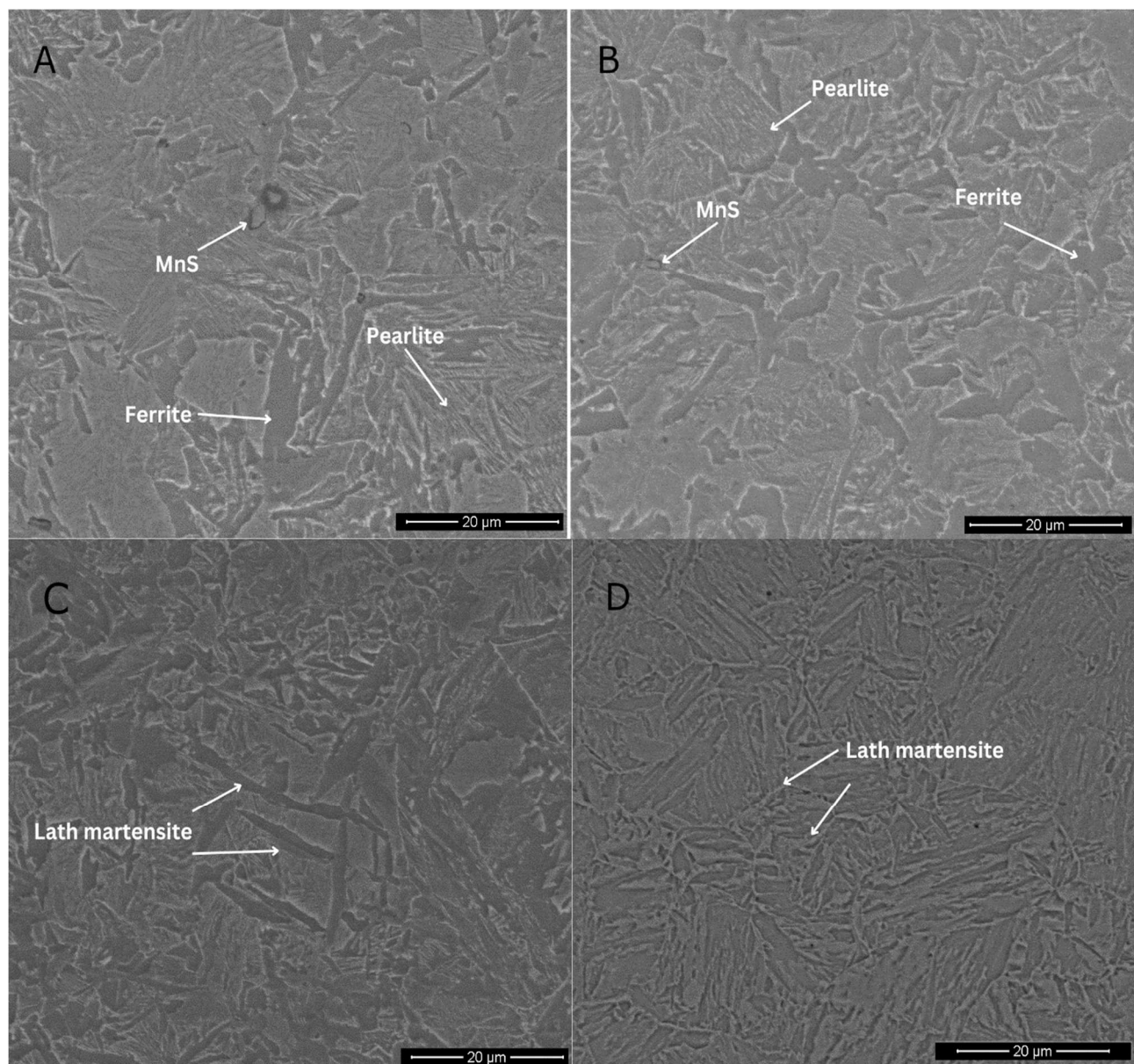
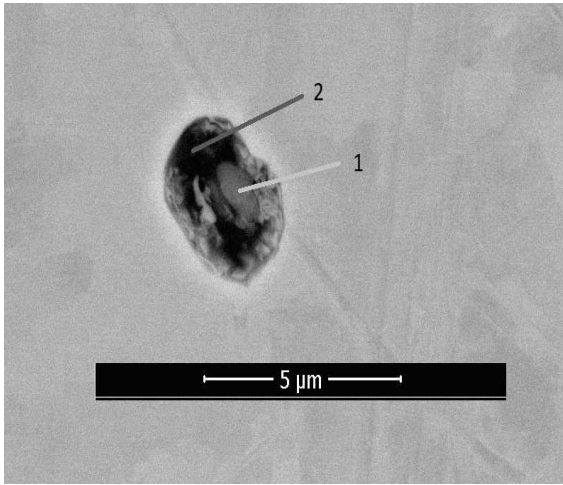


**Fig. 5** SEM micrographs of the core and the surface of TMT rebar before and after artificial aging. (A) and (B) show the core of SNA and SA10 samples, respectively. (C) and (D) show the surface of SNA and SA10 samples, respectively

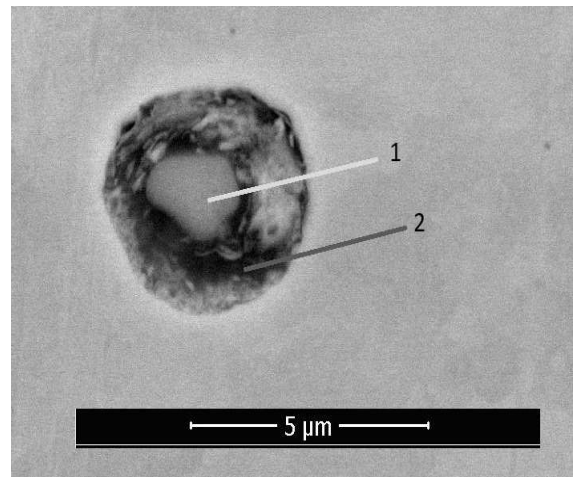
**Tab. 6** EDX analysis of MnS precipitate in the core of SNA sample

Element	Point 1		Point 2	
	Wt. %	At. %	Wt. %	At. %
C	0.8	3.2	1.2	5.0
Si	0.1	0.2	0.1	0.2
P	0	0.0	0.1	0.2
S	14.8	22.5	7.8	12.3
Cr	0.2	0.2	0.2	0.2
Mn	35.6	31.6	17.1	15.7
Fe	48	41.9	72.8	65.8
Cu	0.5	0.4	0.7	0.6
Total	100	100	100	100



**Tab. 7** EDX analysis of MnS precipitate in the core of SA10 sample

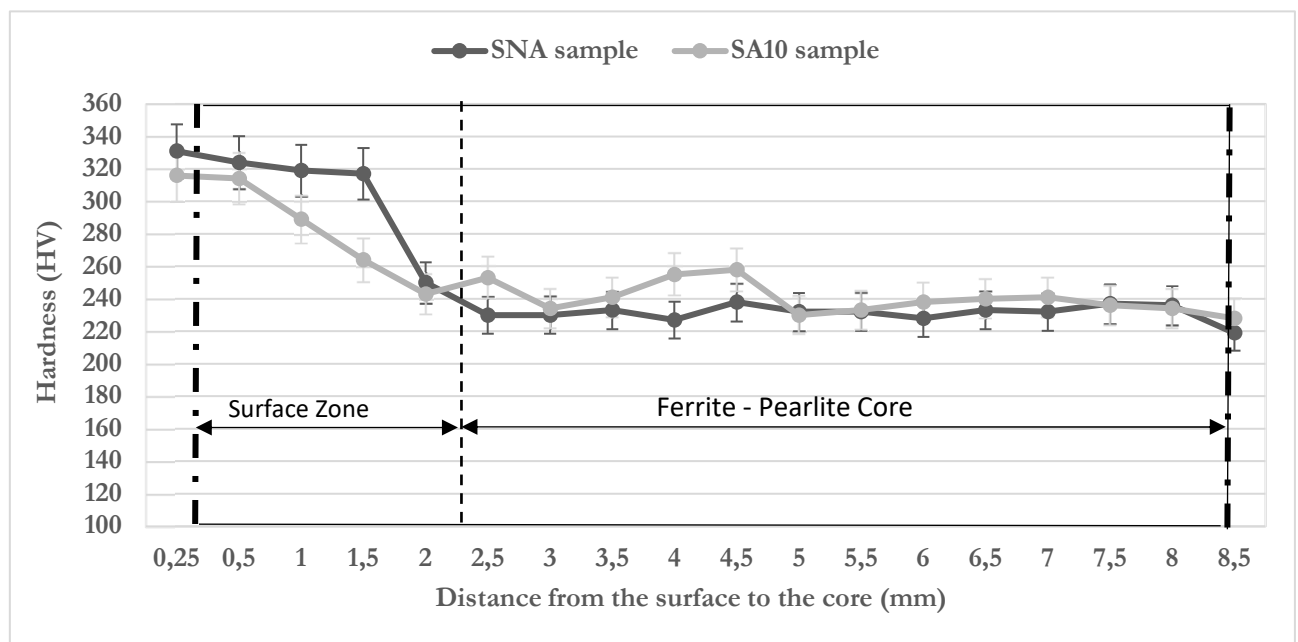
Element	Point 1		Point 2	
	Wt. %	At. %	Wt. %	At. %
<b>C</b>	0.8	3.2	3.6	14.0
<b>Si</b>	0.2	0.3	0.1	0.2
<b>P</b>	0	0.0	0.1	0.2
<b>S</b>	14.7	22.4	7.9	11.5
<b>Cr</b>	0.3	0.3	0.2	0.2
<b>Mn</b>	35.4	31.4	21.7	18.5
<b>Fe</b>	48.1	42.0	65.8	55.1
<b>Cu</b>	0.5	0.4	0.6	0.4
<b>Total</b>	100	100	100	100



### 3.2.5 Microhardness

The hardness profiles along SNA and SA10 samples are plotted in the same figure, figure 6. The hardness of the two samples decreases from the surface of the rebar into the core, indicating the changes of the microstructure. The hardness values of the surface layer down to 2 mm into the core are high and comply

with that expected for tempered martensite. The hardness values beyond 2 mm from the surface are relatively low, corresponding to the predicted values of ferrite and pearlite zone. In general, the surface zone of SNA sample shows more hardness than that of SA10 sample, while the hardness of the core of SA10 sample is slightly greater than that of SNA sample.

**Fig. 6** Hardness profile of SNA and SA10 samples

## 4 Discussion

For all sizes (from 10mm to 25mm) at ageing in bundle, the yield and tensile strength decrease while elongation increases. The change in strength values due to ageing in relatively small sizes (10, 12 mm) was greater than that for larger ones because the self-tempering temperature for small sizes is greater than that for large sizes to produce the same mechanical properties.

In the artificial ageing experiment for size 18mm, the yield and tensile strength decrease while elongation increases due to ageing. There is a good agreement between the results of the ageing in bundles and artificial ageing. The decrease in yield strength at the first two hours of ageing is greater than the decrease in the subsequent ageing intervals. SNA sample is rapidly tempered whereas SA10 sample is slowly tempered. The microhardness of tempered martensite of SNA sample is greater than that of SA10 since rapid tempering



preserves much dislocation density compared with slow tempering as concluded by Saha et al. [32]. The majority of high dislocation density in tempered martensite before ageing was recovered in the two hours of ageing.

JMat-Pro software predicts the phases and precipitates at the equilibrium state, so the phase and precipitates in the core of TMT steel rebar can be predicted due to the slow cooling. The ageing makes the cooling rate slower. SA10 sample has a slower cooling rate than that of SNA sample. So Mn<sub>7</sub>C<sub>3</sub> formation and cementite decomposition have been further occurred in SA10 sample as the ageing process provides more time and temperature for the diffusion of carbon atoms to combine with manganese around MnS precipitates as verified from EDX results, table 6 and table 7.

The prediction of tempered martensite yield strength through JMat-Pro software showed that the tempering/ageing temperature and time affect the yield strength. Increasing tempering temperature decreases the yield and tensile strength. Also increasing tempering time decreases the yield and tensile strength. SNA sample, which undergoes higher cooling rate, is predicted to have a higher yield strength. That prediction can be verified by the microhardness

results of the surface layer of SNA and SA10 samples as shown from figure 6. From the prediction of the equilibrium phases and precipitates formed in the core, the wt. % of cementite decreases from 4.46 % at 400 °C to reach 2.81 % at 50 °C whereas the metal carbide (M<sub>7</sub>C<sub>3</sub>) starts to form at 384 °C to reach 1.28% at 50 °C. Both the decrease in cementite and the increase in M<sub>7</sub>C<sub>3</sub> occur simultaneously. This means that M<sub>7</sub>C<sub>3</sub> forms at the expense of the cementite decomposition. Mn is found to be the major component of the metal carbide, M<sub>7</sub>C<sub>3</sub>.

The distribution of Mn and C in all phases through slow cooling from 400 °C to room temperature is shown in Figure 7 and Figure 8. The cementite has nearly 80 % and 99% of the total Mn and C respectively at 384 °C and these percentages decrease to nearly 15% and 64% at 50 °C. Such decrease of Mn and C in cementite through slow cooling is corresponding to their increase in M<sub>7</sub>C<sub>3</sub> as shown in Figure 7 and Figure 8. Thus, we can predict that C and Mn leave the cementite and form Mn<sub>7</sub>C<sub>3</sub> leading to cementite decomposition and Mn<sub>7</sub>C<sub>3</sub> formation. This prediction can be verified from the EDX results shown in table 6 and table 7, as both C and Mn contents around MnS precipitates increase with ageing forming Mn<sub>7</sub>C<sub>3</sub>.

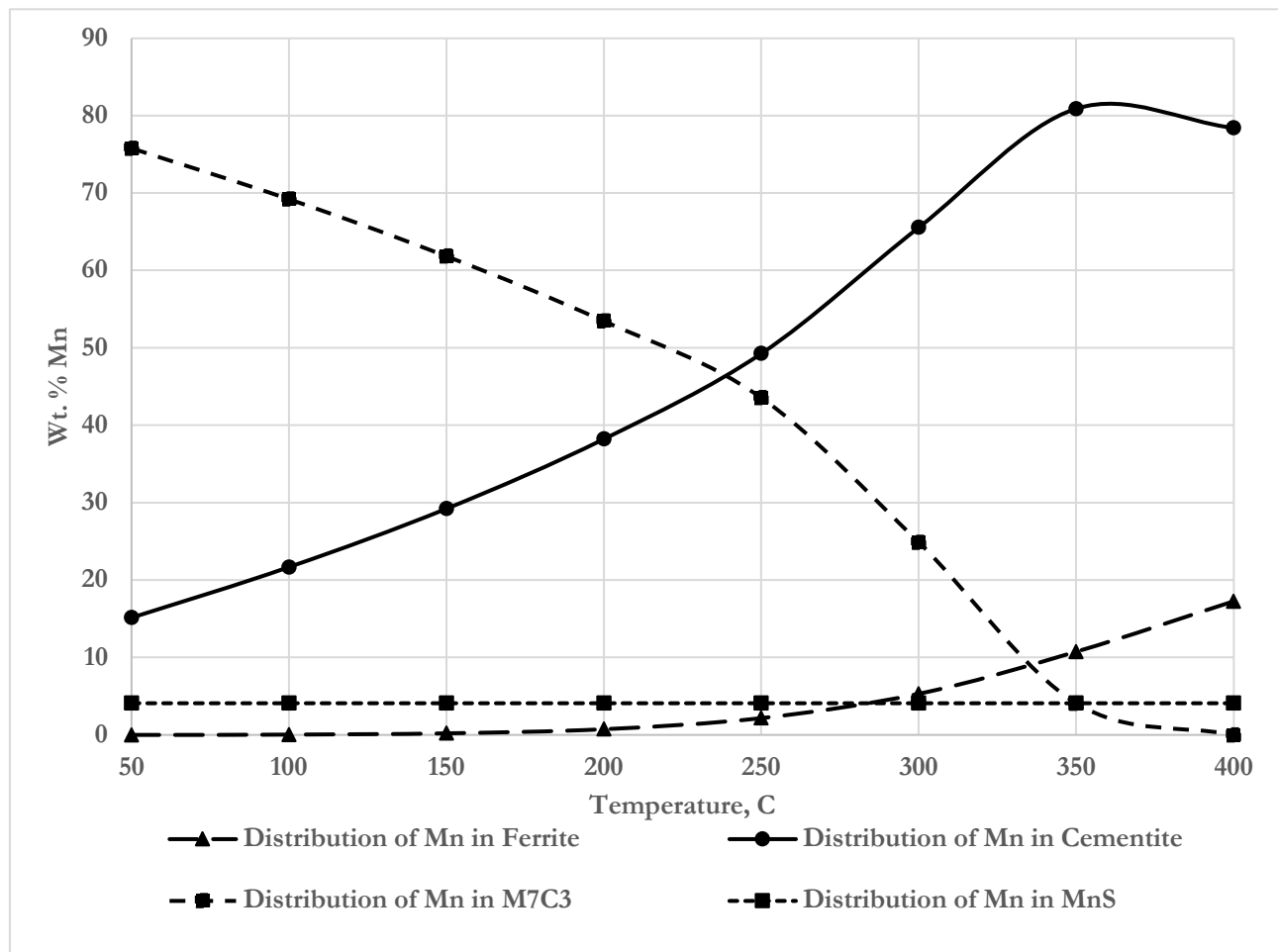


**Fig. 7** The distribution of Mn in all phases and precipitates through slow cooling

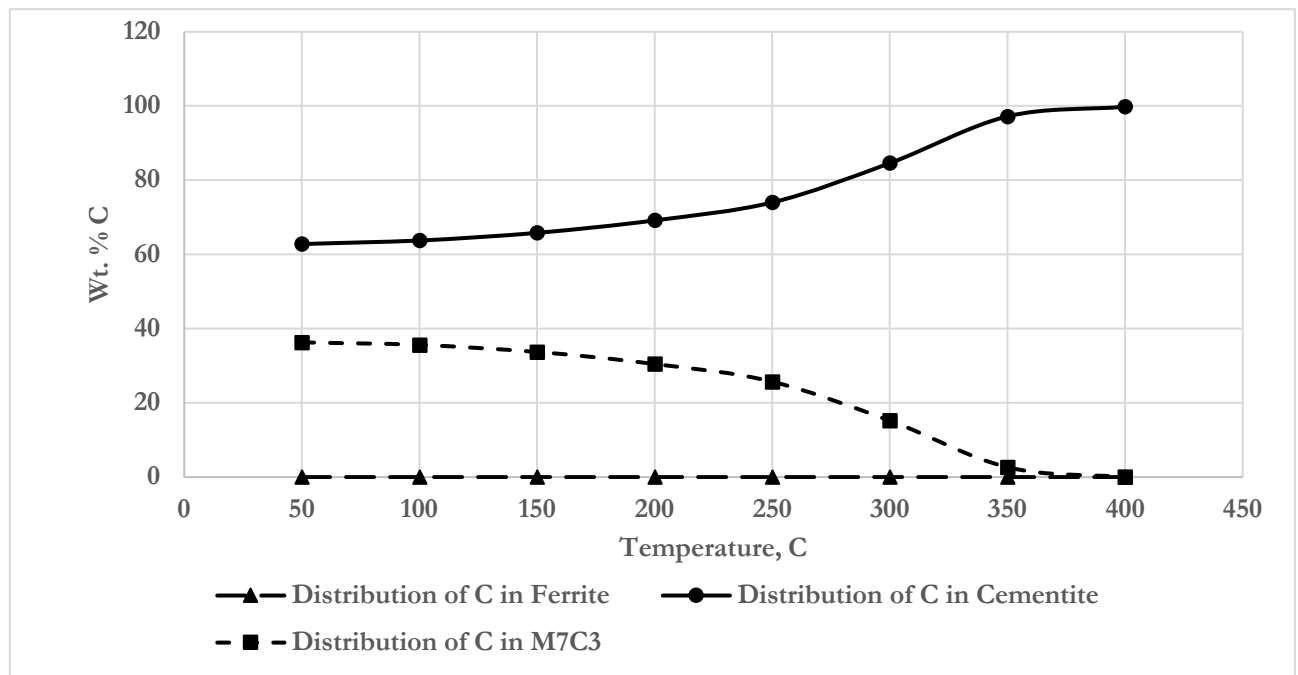


**Fig. 8** The distribution of C in all phases and precipitates during slow cooling

The formation of  $Mn_7C_3$  around MnS precipitates can lead to the following paradox:

- Increasing the strength of the core as the formation of  $Mn_7C_3$  enlarges MnS precipitate size which can hinder the dislocations movement [33].
- Decreasing the strength as a result of the cementite decomposition with ageing while being depleted of C and Mn to form  $Mn_7C_3$ .

The net of the two opposite effects resulted in a slight increase in the strength of the core after ageing which is evident from the measured microhardness profile.

The prediction of the yield strength of tempered martensite formed in the surface of TMT steel rebar shows its decrease with the temperature and the time of tempering /ageing. This was also verified by the microhardness results showing the surface hardness decreasing with ageing.

## 5 Conclusion

- The yield strength and tensile strength decrease by 6.3% and 2.1% respectively with the artificial ageing of TMT rebar steel at 200 °C for 10 hours at heat treatment furnace.
- The elongation and tensile to yield ratio increase by 17.6% and 4.8% respectively with the artificial ageing of TMT rebar steel at 200 °C for 10 hours at heat treatment furnace.

- The decrease in yield strength is greater than that in tensile strength as the yield depends on cooling /heating more than chemical composition on the other side the tensile strength depends on chemical composition more than the cooling /heating rate.
- The artificial ageing of TMT rebar steel at 200 °C for 10 hours makes the martensite layer more softened as shown in microhardness results.
- Due to the slow cooling in the core of TMT rebar steel because of ageing, the Manganese leaves the cementite and combines with the carbon to form  $Mn_7C_3$  around MnS precipitates as shown in EDX results.

## 6 Recommendations

- Due to continuous production and the need of a quick decision to adjust the mechanical properties, the effects of ageing phenomenon on TMT rebar steel's mechanical properties must be taken into consideration to avoid the deviation from the specifications of rebar steel grades.
- To fulfil the designed yield strength, means of accelerating cooling of rebar steel before bundling are recommended to minimize the possible effects of ageing.

- The ageing phenomenon may be optimized to increase the elongation and tensile to yield ratio as well as the bendability of rebar steel.

## Acknowledgement

**Authors would like to acknowledge the management of Egyptian steel plant for providing the data for this research. Authors also thank Dr. Sally Hosny, Environmental Engineering Department, Egypt-Japan University of Science and Technology (E-JUST) for her help in using simulation software programs.**

## References

- [1] C. S. PARK, H. J. YI, Y.-T. KIM, S. W. HAN, T. LEE, Y. H. MOON, "Tempcore Process Simulator to Analyze Microstructural Evolution of Quenched and Tempered Rebar," *Applied Sciences*, vol. 9, no. 14, 2019, doi: 10.3390/app9142938.
- [2] Investigation of Mechanical Properties of Accelerated Cooled and Self-Tempered H-Type Structural Sections," *Archives of Metallurgy and Materials*, Sep. 2023, doi: 10.24425/amm.2023.145493.
- [3] Q. MA, L. HUANG, G. DI, Y. WANG, Y. YANG, C. MA, "Effect of microalloying elements on microstructure and properties of quenched and tempered constructional steel," in *IOP Conference Series: Materials Science and Engineering*, Institute of Physics Publishing, Oct. 2017. doi: 10.1088/1757-899X/242/1/012036.
- [4] H. KHALIFA AND A. EL-KADY, "Effects of Vanadium on Structure and Tensile Properties of Tempcore Steel Bars," *Materials Sciences and Applications*, vol. 13, no. 05, pp. 342–357, 2022, doi: 10.4236/msa.2022.135019.
- [5] H. LIU, B. YANG, Y. CHEN, C. LI, C. LIU, "Precipitation Law of Vanadium in Microalloyed Steel and Its Performance Influencing Factors," *Materials*, vol. 15, no. 22, 2022, doi: 10.3390/ma15228146.
- [6] Z. ZENG, C. LI, Z. LI, Y. ZHAI, J. WANG, Z. LIU, "Effect of final cooling temperature on the microstructure and mechanical properties of high-strength anti-seismic rebar," *Mater Res Express*, vol. 8, no. 9, Sep. 2021, doi: 10.1088/2053-1591/ac2529.
- [7] J. GAO, H. YU, K. WANG, J. LU, Z. ZHU, "Enhanced ductility of strong cold-rolled ribbed rebar through intermediate frequency induction heat treatment based on recrystallization," *Mater Des*, vol. 210, p. 110030, 2021, doi: <https://doi.org/10.1016/j.matdes.2021.110030>.
- [8] O. NIÑO, D. MARTINEZ, C. LIZCANO, M. P. GUERRERO-MATA, R. COLÁS, "Study of the Tempcore Process for the Production of High Resistance Reinforcing Rods," *Materials Science Forum*, vol. 537–538, pp. 533–540, Feb. 2007, doi: 10.4028/www.scientific.net/msf.537-538.533.
- [9] I. DEY, P. MANNA, M. YADAV, N. K. TEWARY, J. K. SAHA, S. K. GHOSH, "Study on the Perspective of Mechanical Properties and Corrosion Behaviour of Stainless Steel, Plain and TMT Rebars," in *Stainless Steels*, A. Singh, Ed., Rijeka: IntechOpen, 2021, ch. 9. doi: 10.5772/intechopen.101388.
- [10] S. A. O. NAIR, P. MOHANDOSS, K. RAM, T. ADNAN, R. G. PILLAI, "Mechanical characteristics of Quenched and Self-Tempered (QST or TMT) steel reinforcing bars used in concrete structures," *Constr Build Mater*, vol. 363, p. 129761, 2023, doi: <https://doi.org/10.1016/j.conbuildmat.2022.129761>.
- [11] J. NIKOLAOU, G. D. PAPADIMITRIOU, "Microstructures and mechanical properties after heating of reinforcing 500 MPa class weldable steels produced by various processes (Tempcore, microalloyed with vanadium and work-hardened)," *Constr Build Mater*, vol. 18, pp. 243–254, 2004, [Online]. Available: <https://api.semanticscholar.org/CorpusID:55447765>
- [12] D. J. MARINOS ROSADO, S. B. ROJAS CHÁVEZ, J. AMARO GUTIERREZ, F. H. MAYWORM DE ARAÚJO, J. A. DE CARVALHO, A. Z. MENDIBURU, "Energetic analysis of reheating furnaces in the combustion of coke oven gas, Linz-Donawitz gas and blast furnace gas in the steel industry," *Appl Therm Eng*, vol. 169, p. 114905, 2020, doi: <https://doi.org/10.1016/j.applthermaleng.2020.114905>.
- [13] J. F. NOVILE, "TEMPCORE® , the most convenient process to produce low cost high strength rebars from 8 to 75 mm."
- [14] S. HOSNY, M. A.-H. GEPREEL, M. G. IBRAHIM, A. R. BASSUONY, "Simulation of Tempcore Process for 500 MPa Steel Bars," *Metals and Materials International*, vol. 27, no. 9, pp. 3359–3370, Sep. 2021, doi: 10.1007/s12540-020-00685-x.

- [15] H. JO *et al.*, “Effects of cooling rate during quenching and tempering conditions on microstructures and mechanical properties of carbon steel flange,” *Materials*, vol. 13, no. 18, Sep. 2020, doi: 10.3390/MA13184186.
- [16] M. H. GHALEH, “Effect of cooling rate on quenched & tempered steel rebar properties,” 2011. [Online]. Available: <https://www.researchgate.net/publication/335692351>
- [17] H. KHALIFA, G. M. MEGAHED, R. M. HAMOUDA, M. A. TAHA, “Experimental investigation and simulation of structure and tensile properties of Tempcore treated rebar,” *J Mater Process Technol*, vol. 230, pp. 244–253, 2016, doi: <https://doi.org/10.1016/j.jmatprotec.2015.11.023>.
- [18] M. S. LAKAL, S. B. CHIKALTHANKAR, “Improvement in Yield Strength of Deformed Steel Bar by Quenching Using Taguchi Method.” [Online]. Available: [www.iosrjournals.org](http://www.iosrjournals.org)
- [19] M. OVSIK, M. STANEK, M. BEDNARIK “Heat Treatment of Steel 1.3520: Influence of Temperature and Austenitization Time,” *Manufacturing Technology Journal*, vol. 24, no. 1, pp. 110–116, 2024, doi: 10.21062/mft.2024.017.
- [20] M. Z. S. HAMEED *et al.*, “Parameter Identification for Thermo-Mechanical Constitutive Modeling to Describe Process-Induced Residual Stresses and Phase Transformations in Low-Carbon Steels,” *Applied Sciences*, vol. 11, no. 2, 2021, doi: 10.3390/app11020550.
- [21] A. H. NOBARI, S. SERAJZADEH, “Modeling of heat transfer during controlled cooling in hot rod rolling of carbon steels,” *Appl Therm Eng*, vol. 31, no. 4, pp. 487–492, 2011, doi: <https://doi.org/10.1016/j.applthermaleng.2010.10.003>.
- [22] S. N. ABDULLAH, N. SAZALI, “A Mini Review on Low Carbon Steel in Rapid Cooling Process,” *Journal of Advanced Research in Applied Mechanics Journal homepage*, vol. 63, pp. 16–22, 2019, [Online]. Available: [www.akademiabaru.com/aram.html](http://www.akademiabaru.com/aram.html)
- [23] H. C. B. ETINEL, O. OZYI GIT, O. OZSOYELLER, “Artificial neural networks modeling of mechanical property and microstructure evolution in the Tempcore process.” [Online]. Available: [www.elsevier.com/locate/compstruc](http://www.elsevier.com/locate/compstruc)
- [24] P. SALVETR, J. KOTOUS, Č. DONIK, A. GOKHMAN, Z. NOVÝ, “Possibilities for Improvement of Mechanical Properties of High-Strength Medium-Carbon SiCr Steels,” *Manufacturing Technology Journal*, vol. 23, no. 4, pp. 525–531, 2023, doi: 10.21062/mft.2023.061.
- [25] G. KRAUSS, “5 - Tempering of martensite in carbon steels,” in *Phase Transformations in Steels*, vol. 2, E. Pereloma and D. V Edmonds, Eds., in Woodhead Publishing Series in Metals and Surface Engineering, vol. 2., Woodhead Publishing, 2012, pp. 126–150. doi: <https://doi.org/10.1533/9780857096111.1.126>.
- [26] J. KOTOUS, Z. NOVÝ, P. MOTYČKA, P. SALVETR “Dilatometric Effects Accompanying Phase Transformations during Tempering of Spring Steels,” *Manufacturing Technology Journal*, vol. 24, no. 1, pp. 62–72, 2024, doi: 10.21062/mft.2024.009.
- [27] R. C. THOMSON, M. K. MILLER, “Carbide precipitation in martensite during the early stages of tempering Cr- and Mo-containing low alloy steels,” *Acta Mater*, vol. 46, no. 6, pp. 2203–2213, 1998, doi: [https://doi.org/10.1016/S1359-6454\(97\)00420-5](https://doi.org/10.1016/S1359-6454(97)00420-5).
- [28] M. JUNG, S.-J. LEE, Y.-K. LEE, “Microstructural and Dilatational Changes during Tempering and Tempering Kinetics in Martensitic Medium-Carbon Steel,” *Metallurgical and Materials Transactions A*, vol. 40, no. 3, pp. 551–559, 2009, doi: 10.1007/s11661-008-9756-2.
- [29] G. B. OLSON, *Martensite*. Materials Park, OH: ASM International, 1992.
- [30] N. SAUNDERS, U. K. Z. GUO, X. LI, A. P. MIODOWNIK, J.-PH. SCHILLÉ, “Using JMatPro to model materials properties and behavior,” *JOM*, vol. 55, no. 12, pp. 60–65, 2003, doi: 10.1007/s11837-003-0013-2.
- [31] W. D. CALLISTER, D. G. Rethwisch, “Fundamentals of Materials Science and Engineering,” 2004. [Online]. Available: <https://api.semanticscholar.org/CorpusID:135718126>
- [32] D. C. SAHA, E. BIRO, A. P. GERLICH, Y. ZHOU, “Effects of tempering mode on the structural changes of martensite,” *Materials Science and Engineering: A*, vol. 673, pp. 467–475, 2016, doi: <https://doi.org/10.1016/j.msea.2016.07.092>.
- [33] B. A. SZAJEWSKI, J. C. CRONE, J. KNAP, “Analytic model for the Orowan dislocation-precipitate bypass mechanism,” *Materialia (Oxf)*, vol. 11, Jun. 2020, doi: 10.1016/j.mtla.2020.100671.